Appl Phys B (2011) 102: 659–671
DOI 10.1007/s00340-010-4181-9

Applied Physics B
Lasers and Optics

Fluoranthene laser-induced fluorescence at elevated temperatures and pressures: implications for temperature-imaging diagnostics

M. Kühni · C. Morin · P. Guibert

Received: 16 April 2010 / Published online: 9 September 2010

Abstract The objective of this study is to develop a quantitative measurement of temperature from fluoranthene fluorescence under conditions with elevated temperatures and pressures. Absorption and fluorescence of fluoranthene are studied in a pressure and temperature range of 0.1–4 MPa and 473–873 K for the two excitation wavelengths of 266 and 355 nm. The influence of thermodynamic parameters such as pressure, temperature and gas composition is characterized in a high-pressure and high-temperature facility. When increasing the pressure, the vibrational relaxation mechanisms are favored, which involves an increase of the fluorescence quantum yield. Concerning the temperature effect, the fluorescence decreases with increasing temperature, this is explained by efficient radiative mechanisms of intersystem crossing. The quenching effect is strongly efficient in air, with a fluorescence evolution described by the Stern–Volmer relation. Over the temperature range studied, the fluorescence quantum yield decreases exponentially by two orders of magnitude. From the temperature dependence of fluoranthene fluorescence in different ambient gases for 266 and 355 nm excitation, the potential temperature measurements in homogeneously and inhomogeneously seeded systems are suggested: the single-color detection technique, the single-excitation two-color detection technique and the dual-excitation wavelength technique.

M. Kühni · C. Morin (✉) · P. Guibert
Institut Jean Le Rond d'Alembert—CNRS UMR 7190, Université Pierre et Marie Curie (Paris 6), 2, place de la Gare de Ceinture, 78210 Saint-Cyr-l'Ecole, France
e-mail: celine.morin@upmc.fr
Fax: +33-130854899

1 Introduction

Temperature measurement in IC engines is of great interest when studying the effect of local inhomogeneities on the combustion development and formation of the pollutant. Laser-induced fluorescence (LIF) is a technique frequently employed to obtain two-dimensional imaging of various parameters, such as the fuel concentration and temperature. For quantification of the technique, the fluorescence signal must be characterized spectrally for various experimental conditions of temperature, pressure and gas composition. It is also necessary to select the appropriate tracer which presents a satisfactory temperature sensitivity of absorption and fluorescence spectra according to the excitation wavelength.

In a global and macroscopic balance formulation and for low laser intensity, the fluorescence signal S_f in number of photons collected is given by the following equation and depends on different thermodynamic parameters:

$$S_f = \frac{E}{hc/\lambda}\eta_{\text{opt}}\, dV_c \left[\frac{XP}{kT}\right]\sigma(\lambda, T)\Phi(\lambda, T, P, X) \tag{1}$$

where E is the laser fluence (J/cm^2), (hc/λ) the energy (J) of a photon at the excitation wavelength λ, η_{opt} the overall efficiency of the collection optics $(-)$, dV_c the collection volume (cm^3), σ the molecular absorption cross section of the tracer (cm^2/molecule), Φ the fluorescence quantum yield $(-)$, X the mole fraction $(-)$, P the total pressure (Pa), k the Boltzmann constant (J/K) and T the temperature (K). The bracketed term corresponds to the fluoranthene molecular density (molecule/cm^3).

The theoretical background for the temperature measurement by LIF depends on the experimental conditions, such as a constant total pressure, a homogeneous molar fraction

of tracer or in opposite cases an inhomogeneous distribution of tracer in the studied volume. According to the experimental conditions, three techniques are defined for the temperature measurement by LIF. The first one is developed from a given excitation wavelength. For fixed experimental conditions (energy and excitation wavelength of laser, efficiency of the collection optics, measurement volume), the fluorescence signal is proportional to the tracer concentration, the absorption cross section and the fluorescence quantum yield. When the total pressure is constant and the tracer is distributed homogeneously in the volume, the fluorescence signal presents an evolution in $1/T$:

$$S_f \propto \frac{1}{T}\sigma(\lambda, T)\Phi(\lambda, T, P) \tag{2}$$

In the case of uniform conditions, the single-wavelength (1λ) excitation strategy measured in a single-wavelength band is then sufficient for the temperature measurement.

The second technique is the temperature measurement from a single-excitation wavelength and the fluorescence detection in dual wavelength bands. With an inhomogeneous distribution of tracer and with the use of a single-excitation wavelength, the ratio between the fluorescence signal detected on the spectral bands $\Delta\lambda_1$ and $\Delta\lambda_2$ is expressed by:

$$\frac{S_f^{\Delta\lambda_1}(x, y, T, P)}{S_f^{\Delta\lambda_2}(x, y, T, P)} = \frac{\eta_{\text{opt}}^{\Delta\lambda_1} E(x, y) n_{\text{tracer}}(x, y)\sigma(T(x, y))\phi^{\Delta\lambda_1}(T(x, y), P)}{\eta_{\text{opt}}^{\Delta\lambda_2} E(x, y) n_{\text{tracer}}(x, y)\sigma(T(x, y))\phi^{\Delta\lambda_2}(T(x, y), P)} \tag{3}$$

with $n_{\text{tracer}}(x, y)$ the local tracer concentration.

With equal tracer concentration and laser energy in each point, the ratio of fluorescence signals for both spectral bands depends only on the temperature:

$$\frac{S_f^{\Delta\lambda_1}(x, y, T, P)}{S_f^{\Delta\lambda_2}(x, y, T, P)} \propto \frac{\Phi^{\Delta\lambda_1}(T(x, y))}{\Phi^{\Delta\lambda_2}(T(x, y))} = f\big(T(x, y)\big) \tag{4}$$

The ratio sensitivity depends on the selected spectral wavelength bands $\Delta\lambda_1$ and $\Delta\lambda_2$.

The third technique is developed when the tracer partial pressure varies and the tracer concentration is inhomogeneous, that is the case during the mixing phase in IC engine. The dual-excitation wavelength (2λ) technique is then applied. The temperature measurement is deduced from the ratio of fluorescence signals resulting from a dual-excitation wavelength:

$$\frac{S_{f,\lambda_2} E_{\lambda_1}}{S_{f,\lambda_1} E_{\lambda_2}} \propto \frac{\sigma(\lambda_2, T)\Phi(\lambda_2, T, P)}{\sigma(\lambda_1, T)\Phi(\lambda_1, T, P)} \tag{5}$$

The two laser pulses must present a short temporal delay to ensure separate detection of the LIF signals that are detected in the same wavelength band. The LIF signals must also show different temperature dependence.

The ratios defined in (2), (4) and (5) depend on the pressure and temperature variations of the absorption cross section and the fluorescence quantum yield for the selected tracer. These techniques of temperature measurement require a calibration of the fluorescence signal in a large temperature and pressure domain according to an accurate methodology [1–3]. The single- or dual-excitation wavelengths and the tracer must be chosen to obtain satisfactory signals with different sensitivities according to the temperature and the wavelength collection range. For example, Luong et al. [4] have developed the single-excitation wavelength two-color detection technique based on toluene fluorescence. This technique of a single-laser single-camera imaging was applied to measure in-cylinder temperature distributions in a direct-injection spark-ignition engine with homogeneous charge. Using the spectral calibration data from Koban et al. [5], temperature is extracted from measured fluorescence intensity ratios. Koban et al. have studied the $S_0 \rightarrow S_1(\pi, \pi^*)$ absorption and fluorescence spectra of toluene in the temperature range of 300–1130 K and 300–930 K respectively, at atmospheric pressure in nitrogen and for the excitation wavelengths of 248 and 266 nm.

Fujikawa et al. [6] have investigated the dual-excitation wavelength technique for two-dimensional temperature measurements in an engine from toluene fluorescence. Preliminary work has allowed the combination of the fluorescence tracer between acetone, 3-pentanone, toluene and the pair of the excitation wavelengths between 248, 266 and 308 nm to be defined. For this study, carried out in a heated and pressurized constant volume vessel, the combination of toluene and the dual-excitation wavelengths 266/248 nm has been applied in an engine.

A similar technique (with a single-excitation wavelength and a "red" and "blue" fluorescence ratio) was used by Kaiser et al. [7] to simultaneously measure temperature and equivalence ratio with naphthalene as tracer for diesel-like fuels and fuel surrogates. An increase of temperature and oxygen concentrations leads to a broadening of the fluorescence spectrum of 5% naphthalene in dodecane and a red-shift. From the temperature calibration curves obtained from two-color imaging of a heated jet, the equivalence ratio and temperature images were obtained from the two-color PLIF method applied in a mesoscale burner. Before applying the dual-excitation wavelength technique, Thurber [8] studied the temperature dependence of acetone fluorescence at different excitation wavelengths and atmospheric pressure in nitrogen between 300 and 1000 K. He defined optimal wavelengths for measurements of temperature. The excitation wavelength of 248 or 266 nm is suitable for a

Table 1 Experimental conditions for the temperature measurement by LIF from the single or dual-excitation wavelength technique

Reference	λ_{exc} [nm]	Tracer	Ambient gas	Temperature and pressure range	Application
Einecke et al. [3]	248 308	3-Pentanone	Air	$350 < T < 600$ K	2λ-excitation technique (308/248 nm) Two-stroke engine
Luong et al. [4]	248	Toluene	Air	$300 < T < 675$ K	1λ-excitation technique and detection in dual wavelength bands Direct-injection spark-ignition engine
Koban et al. [5]	248 266	Toluene	N_2	$373 < T < 930$ K $P = 0.1$ MPa	1λ-excitation technique and detection in dual wavelength bands Shock tube; Heated flow-cell
Fujikawa et al. [6]	248 266	Toluene	Air	$373 < T < 523$ K $0.1 < P < 1$ MPa	2λ-excitation technique (266/248 nm) Spark-ignition engine
Kaiser et al. [7]	266	Naphtalene	N_2 O_2	$400 < T < 928$ K $P = 0.1$ MPa	1λ-excitation technique and detection in dual wavelength bands Mesoscale burner
Koch [9]	248 266 308	3-Pentanone	N_2	$300 < T < 1000$ K $0.1 < P < 0.6$ MPa	2λ-excitation technique (308/266 nm) Heated turbulent jet
Thurber et al. [10, 11]	248, 266, 276, 282, 289, 300, 308, 320	Acetone	N_2	$300 < T < 1000$ K $P = 0.1$ MPa	2λ-excitation technique (308/248 nm) 1λ-excitation technique (248 nm) Heated jet
Grossmann et al. [12]	248 277 312	Acetone 3-pentanone	N_2 O_2 Air	$T = 383$ K, $P = 0.1-5$ MPa and $T = 383-573$ K, $P = 0.1$	2λ-excitation technique (312/248 nm) Heatable high-pressure cell

single-wavelength temperature measurement, while dual-excitation wavelength diagnostic with the 308/248 nm or 308/266 nm fluorescence ratio is attractive. Simultaneous quantitative imaging of temperature and mixture fraction with the 308/248 nm wavelength pair has been investigated in a heated turbulent jet. Koch [9] has shown that for similar excitation wavelengths, 3-pentanone's temperature sensitivity is superior to that of acetone. Temperature fields were measured in a heated turbulent jet by using the 308/266 nm excitation.

Table 1 summarizes the studies carried out for the temperature measurement by LIF according to the excitation wavelength, the tracer, the ambient gas, the pressure and temperature range.

As shown in Table 1, ketones, aromatic molecules and polycyclic aromatic hydrocarbons (PAHs) are the current tracers of non-fluorescing fuels used for measurements of temperature by LIF, for the following conditions: at atmospheric pressure in a large range of temperature or at low temperature in a large range of pressure. For measurements of temperature from the dual-excitation wavelength technique, different lasers are used, essentially Nd:YAG—dye laser combination to produce specific excitation wavelengths from 266 to 320 nm, which requires a flexible beam delivery system.

The objective of the present work is to investigate a new combination of a fluorescence tracer, fluoranthene and the pair of 266 and 355 nm excitations accessible from pulsed lasers under conditions with elevated temperatures and pressures, as is the case in an IC engine, for imaging temperature. Fluoranthene fluorescence can also provide information on PAHs formation, soot precursors during combustion. For a given excitation wavelength, the dependence of the fluoranthene fluorescence signal with parameters such as pressure, temperature, gas composition is characterized by experiments investigated in a high-pressure and high-temperature constant volume vessel. The parameters influencing the fluoranthene fluorescence are studied to define the most appropriate technique of temperature measurement according to the experimental conditions. Finally the potential temperature measurements on fluoranthene fluorescence are presented.

2 Experimental

Absorption and fluorescence experiments in vapor phase are conducted in a high-pressure and high-temperature (HP–HT) facility described in detail in [13] (cf. Fig. 1). The maximum studied temperature is 873 K and the maximum pressure is 4 MPa. The liquid solution is injected via a syringe linked to a capillary tube into the chamber heated by electrical resistances (cell volume of 7.6969×10^{-4} m^3). The liquid solution is vaporized by reaching the boiling point and

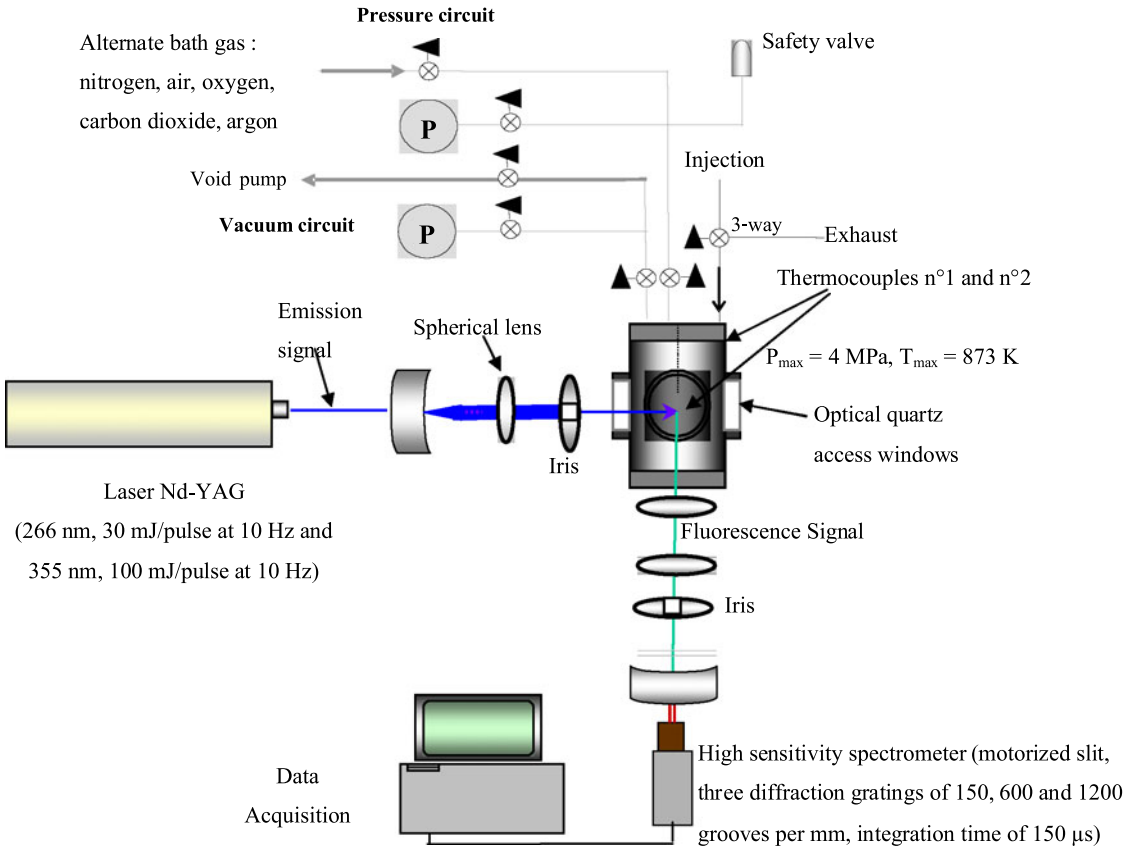

Fig. 1 High-pressure and high-temperature facility with optical system for temperature measurements

vapor pressure through a vacuum pump. Temperature homogeneity is controlled inside the facility by three thermocouples. The optical system described in Fig. 1 is composed of a frequency-quadrupled pulsed Nd:YAG laser (266 nm—30 mJ/pulse at 10 Hz and 355 nm—100 mJ/pulse at 10 Hz). The pulse width is contained between 2–3 nm at 355 nm with an energy stability of ±4% and between 3–4 nm at 266 nm with an energy stability of ±8%. The line width is less than 1 cm^{-1}, the intensity is 0.1×10^{-3} $W{\cdot}s^{-1}{\cdot}cm^{-2}$. The UV beam is centered in the HP–HT chamber by a focusing lens system. The fluorescence signal is collected from spherical lens along the axis perpendicular to the incident light beam through optical quartz access windows. It is analyzed by a high-sensitivity spectrometer (motorized slit, three diffraction gratings of 150, 600 and 1200 grooves per mm, integration time of 150 µs). For given experimental conditions of pressure and temperature, the fluorescence signals are averaged from 100 emission spectra registered with back noise, reference spectrum and an integration time of 150 µs, which corresponds to a total residence time of the fluoranthene sample of 20 s. Every experiment is reproduced three times.

To select the appropriate tracer for this work, the fluorescence spectra are firstly measured for different tracers (polycyclic aromatic hydrocarbons PAHs: naphthalene $C_{10}H_8$, anthracene $C_{14}H_{10}$, pyrene and fluoranthene $C_{16}H_{10}$, aromatics: toluene C_7H_8, ketones: 3-pentanone $C_5H_{10}O$, acetone C_3H_6O) at 573 K and 0.1 MPa, in nitrogen, for the two excitation wavelengths of 266 and 355 nm. The tested fluorescent tracers present very low fluorescence signal for the excitation wavelength of 355 nm, except anthracene, which has a lower fluorescence intensity relative to that of fluoranthene (cf. Fig. 2).

Fluoranthene is then chosen as tracer for its spectroscopic properties: satisfactory fluorescence signals for the large studied temperature and pressure range for the two excitation wavelengths of 266 and 355 nm and for its chemical stability at high temperature. No information is available on the variation of fluoranthene fluorescence in a large pressure and temperature range. However there is data available for toluene for visualizing mixing processes and for quantitative imaging of temperature [4–6]. The temperature effect on the fluorescence spectrum of PAHs was studied, but not on the fluorescence signals. For example, Kaiser and Long [7] have carried out a spectral study of naphthalene and 1-methylnaphtalene fluorescence, where a spectral broadening and red-shift are underlined when increasing temperature and oxygen concentration. Similar results have been

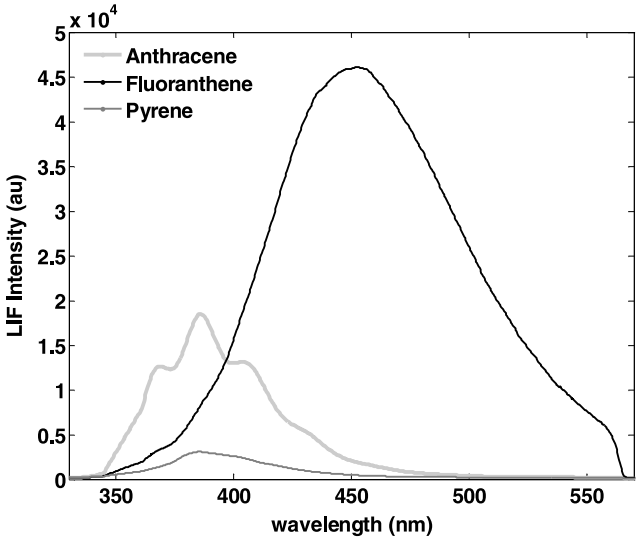

Fig. 2 Comparison of fluorescence spectra for different PAHs excited at 355 nm in nitrogen for a pressure of 0.1 MPa and a temperature of 573 K

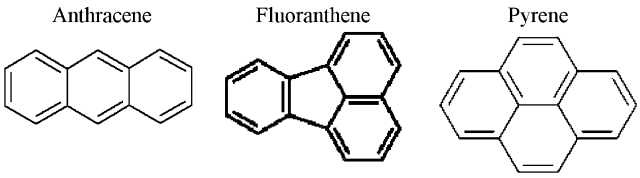

found by Ossler et al. [14] who have studied picosecond laser-induced fluorescence from gas-phase naphthalene, fluorine, anthracene and pyrene, with a recording of the fluorescence emission resolved temporally. The results concern the temperature dependence of temporal spectral profiles and of the lifetime, where a broadening of the profiles is observed when increasing temperature.

Fluoranthene is a PAH which incorporates a five-membered, cyclopentadienyl ring in its structure. As it is a solid component, fluoranthene is weighed in a pair of scales with a precision of 10^{-4} g and then is dissolved in iso-octane (C_8H_{18}). The obtained solutions show a satisfactory dissolution and are changed regularly to avoid the decomposition and polymerization of fluoranthene in the presence of impurities. Experiments show that iso-octane does not fluoresce when excited at 266 and 355 nm. To characterize the eventual interactions between fluoranthene and iso-octane in the gas phase, the collision frequencies (k_{vib}) between the fluoranthene and iso-octane molecules are calculated by the following equation [13]:

$$k_{\text{vib}} = \left(\frac{X_M P}{kT}\right) Z_{\text{coll}} \tag{6}$$

where X_M is the partner mole fraction (fluoranthene or iso-octane), P the total pressure (Pa), T the temperature (K), k the Boltzmann constant (J/K) and Z_{coll} the Lennard–Jones collision frequency ($\text{cm}^3 \cdot \text{s}^{-1}$).

For example, at 0.1 MPa and 473 K, the calculated collision frequencies are the following:

$$k_{\text{vib}}^{C_{16}H_{10}/N_2} = 2.634 \times 10^{10}\ \text{s}^{-1}$$
$$k_{\text{vib}}^{C_{16}H_{10}/C_8H_{18}} = 4.806 \times 10^{9}\ \text{s}^{-1}$$

In the gas phase where the experiments are conducted, the collision frequencies between fluoranthene and iso-octane are low, the interaction between the two molecules can then be neglected. Moreover, fluoranthene does not pyrolyze in the temperature range explored [15]. The use of a fluoranthene—iso-octane solution will not affect the environment of the engine.

The experiments in the HP-HT facility are conducted in nitrogen, argon, carbon dioxide and air, for a pressure and temperature range of 0.1–4 MPa and 473–873 K. For given experimental conditions of pressure and temperature, the fluorescence signals are averaged from 100 emission spectra. Every experiment is reproduced three times. The normalized standard deviations are included for the excitation wavelength of 266 nm between 1.3–9.7% in nitrogen, 0.3–11.9% in argon and 0.3–12.5% in carbon dioxide. For the excitation wavelength of 355 nm, the normalized standard deviations are: 1.4–12.5% in nitrogen, 0.3–12.1% in argon, and 0.7–11.5% in carbon dioxide.

3 Results and discussion

3.1 Fluoranthene absorption and fluorescence

An understanding of the variation of the absorption cross section with temperature and excitation wavelength is required for quantitative measurements of temperature by LIF. A deuterium lamp coupled to an optical fiber is used for the measurements of absorption cross section σ deduced from Lambert–Beer's law (cf. Fig. 3a):

$$\sigma(\lambda) = \frac{\ln[I_0(\lambda)/I(\lambda)]}{lC} \tag{7}$$

with I_0 the incident intensity, I the transmitted intensity, l the path length and C the fluoranthene concentration. The two intensities are measured directly from the spectrometer with a spectral resolution of 0.355 nm.

As shown in Fig. 3b, the normalized absorption cross section shows a steady rise with temperature, with the effect increasing at 355 nm. This may be explained by the increasing of the ground state vibrational energy with temperature. The absorption cross section increases linearly by 1.5% per degree for the excitation wavelength of 266 nm and by 3.5%

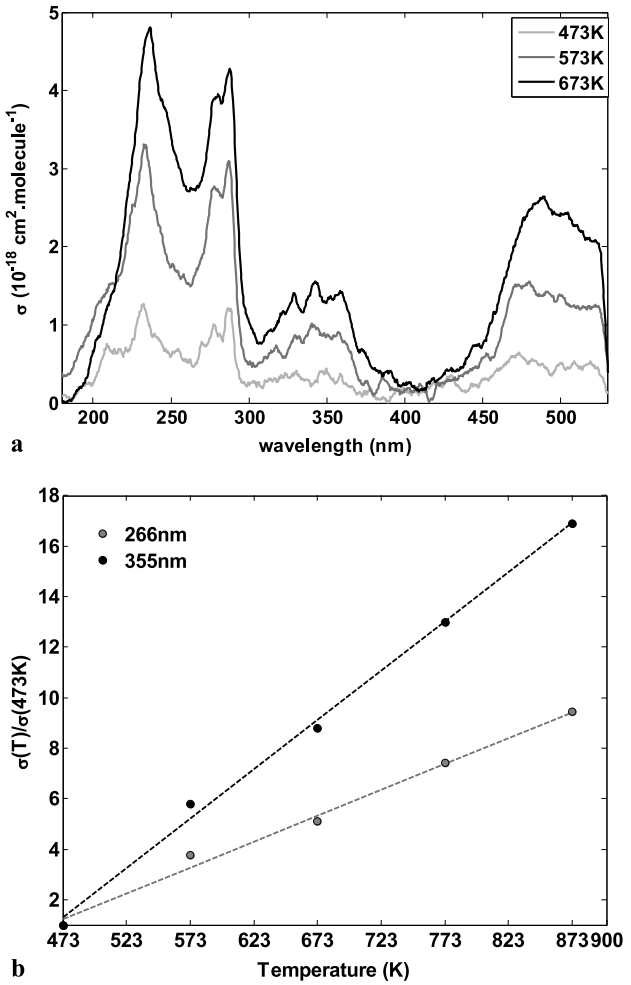

Fig. 3 Absorption cross section of fluoranthene in nitrogen at 0.2 MPa for three temperatures (**a**) and evolution of the normalized absorption cross section of fluoranthene versus temperature in nitrogen for the two excitation wavelengths of 266 and 355 nm (**b**). The absorption cross section is normalized to the reference value at 473 K

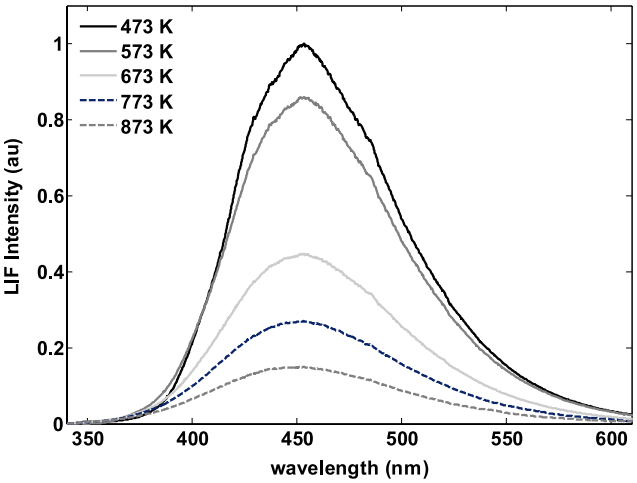

Fig. 4 Fluorescence spectra of fluoranthene for different temperatures and a pressure of 1.2 MPa in nitrogen ($\lambda = 355$ nm). Each spectrum is normalized to the maximum value of the fluorescence spectrum recorded at 473 K

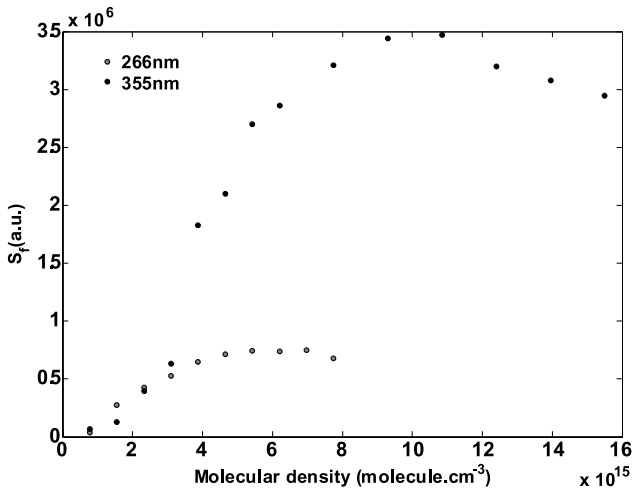

Fig. 5 Evolution of fluoranthene fluorescence signal versus molecular density in nitrogen at 0.2 MPa and 573 K for the two excitation wavelengths

per degree at 355 nm. To underline the influence of temperature on fluorescence intensity, the fluorescence signal will then be normalized by the value of the absorption cross section for a given temperature.

Fluoranthene fluorescence experiments are investigated in the linear fluorescence regime, with an intensity of the incident laser much lower than the saturation intensity, i.e. an energy of 8 mJ. The laser energies vary between 7.5 and 8.8 mJ, which sets a normalization of the results by the respective value of the laser energy. The percentage of laser absorption is included between 5–8% according to the ambient gas.

As represented in Fig. 4, fluoranthene in iso-octane presents a fluorescence emission band between 380–600 nm with a peak at 450 nm that corresponds to the fluorescence band $S_1 \rightarrow S_0$. The excitation wavelength has no influence on the fluorescence peak and the spectral emission domain. Philen and Hedges [16] have characterized the first two excited singlet states of fluoranthene. The S_1 fluorescence occurs over the region from 405 nm to approximately 540 nm with a lifetime of 58 ns, while the S_2 fluorescence occurs in the region from 370 to 395 nm with a lifetime of 143 ns. Bark and Forcé [17] have observed similar fluoranthene fluorescence spectra between 400 and 600 nm in various environments, in different solvents, temperatures, in the solid and vapor phase. They have underlined that the emission maximum was independent of environment, as observed in this work.

The influence of the tracer molecular density is presented in Fig. 5. The fluorescence signal increases with increasing fluoranthene molecular density to reach a maximum value: 10^{16} molecules·cm^{-3} for the excitation wavelength

of 355 nm and 6×10^{15} molecules·cm^{-3} at 266 nm. Beyond these values, the fluorescence signal decreases slightly, which is due to two quenching processes, reabsorption and self-quenching (collisions with fluoranthene molecules at the fundamental state that involves the formation of an excimer). Therefore to avoid these phenomena, the volume of fluoranthene—iso-octane is fixed to 400 µL with 2 g/L of fluoranthene, which corresponds to a molecular density of 3.099×10^{15} molecules·cm^{-3}.

3.2 Pressure dependence

The influence of pressure on fluorescence intensity is characterized by studying the fluorescence signal normalized to the molecular density and the reference value at 0.1 MPa noted S_f^* or the fluorescence signal normalized to the molar fraction and the reference value at 0.1 MPa noted S_f^+. At fixed temperature and wavelength, the signal S_f^* is proportional to the fluorescence quantum yield and the signal S_f^+ to the pressure and the fluorescence quantum yield. The evolution of the signals S_f^+ allows the influence of pressure on fluorescence to be more underlined, according to the temperature.

For the interpretation of the plotted curves, the signals are normalized to the reference value at 0.1 MPa:

$$\frac{S_f^*(P)}{S_f^*(P_{\text{ref}})} \propto \left[\frac{\Phi(\lambda, T, P)}{\Phi(\lambda, T, P_{\text{ref}})}\right] \tag{8}$$

$$\frac{S_f^+(P)}{S_f^+(P_{\text{ref}})} \propto \left[\frac{P}{P_{\text{ref}}}\right]\left[\frac{\Phi(\lambda, T, P)}{\Phi(\lambda, T, P_{\text{ref}})}\right] \tag{9}$$

As pictured in Fig. 6, the fluorescence signal increases with pressure between 0.1 and 1.5 MPa, then reaches a constant value up to 4 MPa or increases slightly according to the different temperatures and the two excitation wavelengths. When increasing the pressure, the vibrational relaxation mechanisms are favored and the low-energy excited levels with high-fluorescence quantum yield are rapidly reached. Between 0.1 and 1.5 MPa, the increase of fluorescence with pressure is then important. From a pressure of 1.5 MPa, the fluorescence increases slightly up to 4 MPa or presents a constant value at 473 K characterized by an important energy of vibrational states. It corresponds to the pressure limit of complete vibrational relaxation. From a pressure of 1.5 MPa, the pressure increase does not emphasize the process of vibrational relaxation. Similar trends are observed for ketones for limited ranges of temperature and pressure [12, 13]. However, it must be underlined that we have a non-monotonous behavior of the data obtained at high temperature, when compared to the best curve fitted for low pressures. This can be explained by higher normalized standard deviations at elevated temperature. For example, at

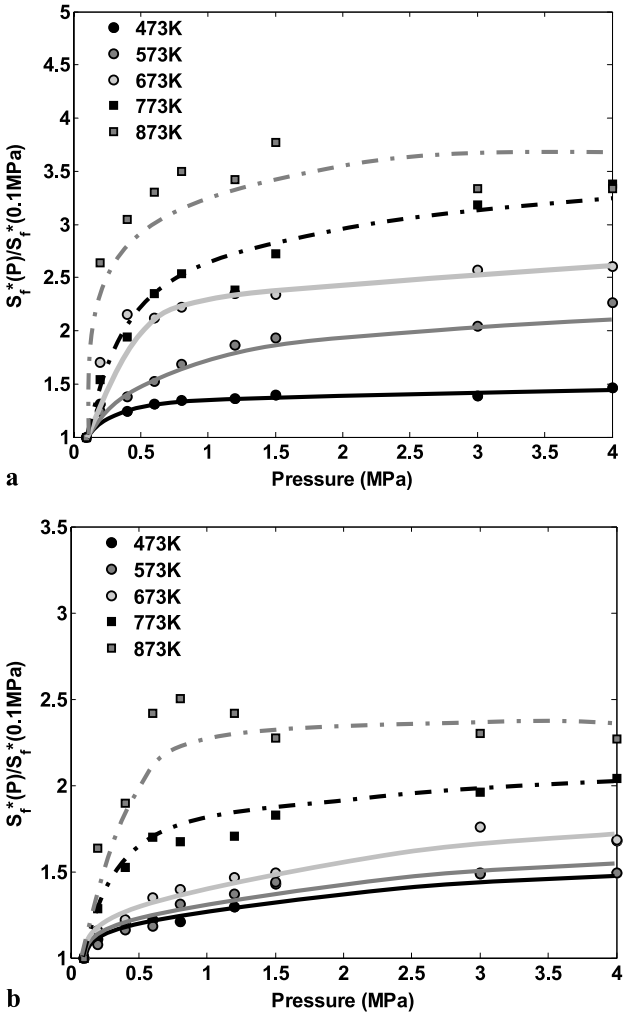

Fig. 6 Influence of pressure on fluoranthene fluorescence excited at 266 nm (**a**) and 355 nm (**b**), in nitrogen for different temperatures. The signal S_f^* is normalized to the molecular density and the reference value at 0.1 MPa

3 MPa and for the excitation wavelength of 266 nm, the normalized standard deviation is 8.2% at 873 K against 1.5% at 473 K.

The influence of the pressure on fluoranthene fluorescence is more marked at high temperature and for the excitation wavelength of 266 nm. The vibrational relaxation mechanism is then more important at high temperature and for the excitation wavelength of 266 nm. Figure 7 presents this result with a quasi-linear evolution of the fluorescence signal normalized to the molar fraction in nitrogen. However, the temperature effect is only marked from a pressure of 0.8 MPa. For the studied pressure range, at 473 K, the signal S_f^+ is increased by 50% for the excitation wavelength of 355 nm and 60% at 266 nm, against at 873 K the increase of 80% for the excitation wavelength of 355 nm and 130% at 266 nm.

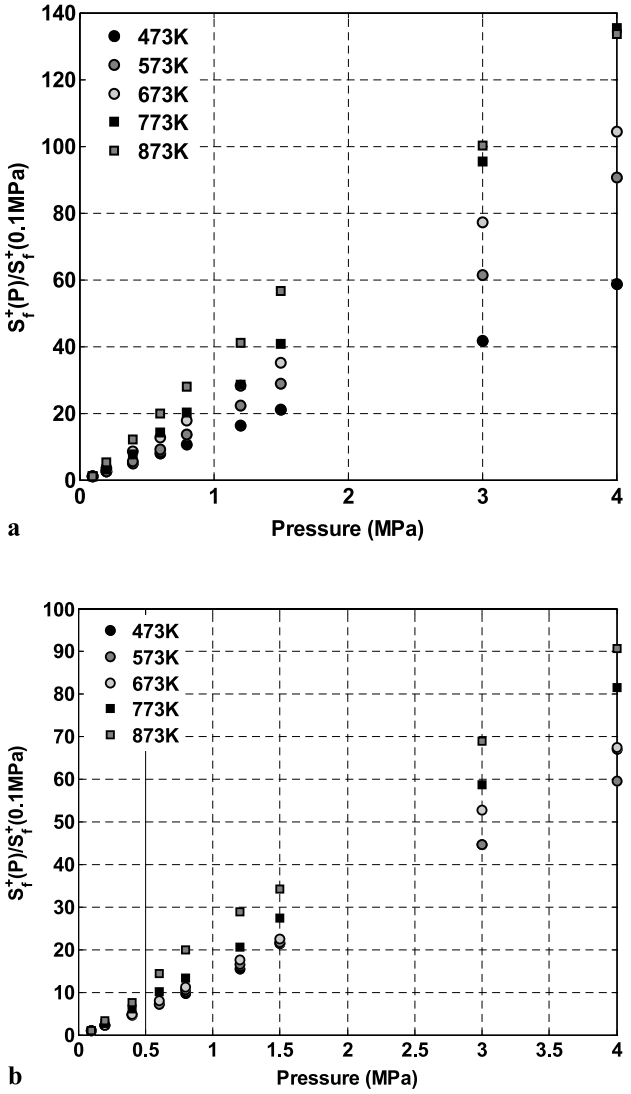

Fig. 7 Influence of pressure on fluoranthene fluorescence excited at 266 nm (**a**) and 355 nm (**b**), in nitrogen for different temperatures. The signal S_f^+ is normalized to the molar fraction and the reference value at 0.1 MPa

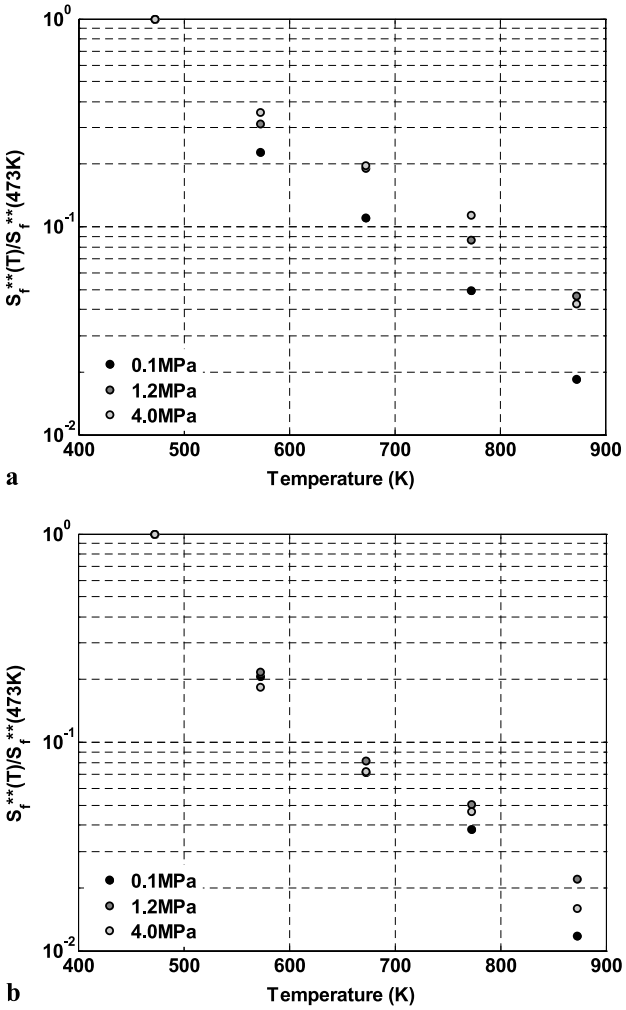

Fig. 8 Influence of temperature on fluoranthene fluorescence excited at 266 nm (**a**) and 355 nm (**b**) in nitrogen for different pressures. The signal S_f^{**} is normalized to the molecular density, the absorption cross section and the reference value at 473 K

3.3 Temperature dependence

As the fluoranthene absorption cross section is dependent on temperature variations, the fluorescence signals S_f^* and S_f^+ are normalized to the corresponding cross section value for a given temperature and excitation wavelength and are noted S_f^{**} and S_f^{++}. The signal S_f^{**} represents directly the fluorescence quantum yield. The signal S_f^{++} which depends on the inverse of the temperature can be used to convert the fluorescence signal to temperature from the single-color detection technique for the temperature measurement.

For the interpretation of the plotted curves, the signals are normalized to the reference value at 473 K:

$$\frac{S_f^{**}(T)}{S_f^{**}(T_{\text{ref}})} \propto \left[\frac{\Phi(\lambda, T, P)}{\Phi(\lambda, T_{\text{ref}}, P)}\right] \tag{10}$$

$$\frac{S_f^{++}(T)}{S_f^{++}(T_{\text{ref}})} \propto \left[\frac{T_{\text{ref}}}{T}\right]\left[\frac{\Phi(\lambda, T, P)}{\Phi(\lambda, T_{\text{ref}}, P)}\right] \tag{11}$$

The temperature effect on the fluoranthene fluorescence is observed for the two excitation wavelengths in nitrogen for different pressures in Figs. 8 and 9. In our temperature range, the fluorescence quantum yield decreases significantly for the two excitation wavelengths, with a more marked decrease at low pressure. This evolution is similar for all the studied pressures. At 0.1 MPa, the fluorescence quantum yield decreases exponentially by two orders of magnitude

within the studied temperature range, the single exponential fit is given by:

$$\left.\frac{\Phi(T)}{\Phi(473\ \mathrm{K})}\right|_{266\ \mathrm{nm}} = 71.42\exp(-0.0095T) \quad (12)$$

$$\left.\frac{\Phi(T)}{\Phi(473\ \mathrm{K})}\right|_{355\ \mathrm{nm}} = 112.91\exp(-0.0106T) \quad (13)$$

In comparison, Koban et al. [5] have obtained the following exponential fit for the toluene fluorescence quantum yield valid for 1 bar nitrogen bath gas and 300–950 K:

$$\left.\frac{\Phi(T)}{\Phi(296\ \mathrm{K})}\right|_{266\ \mathrm{nm}} = 22.5\exp(-0.0105T) \quad (14)$$

The fluorescence decrease is explained by a vibrational energy increase of the S_1 state, which involves more efficient radiative mechanisms of intersystem crossing. The fluoranthene molecule presents the $\pi \rightarrow \pi^*$ transition characteristic of aromatics. The intersystem crossing is activated between singlet toward triplet levels, lower in energy. However, it is difficult to conclude that the vibrational energy increase involves such magnitude of the fluorescence decrease, as underlined by Koban et al. [5]. By calculating the relative population levels and using the quantum yield data, they found that changes in vibrational energy could not explain the steep signal fall-off; additional lifetime measurements must be investigated for more understanding.

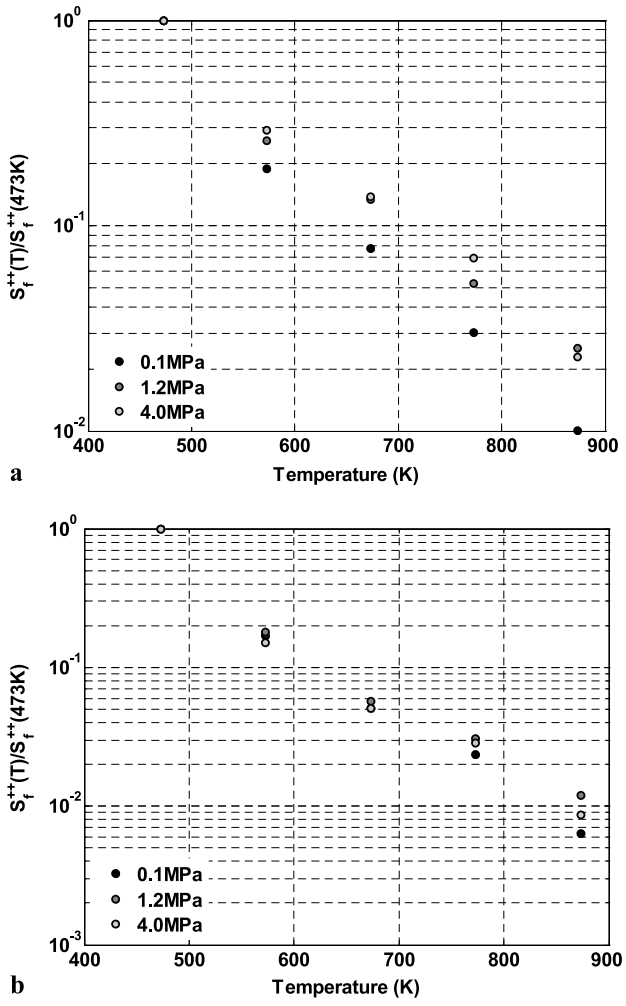

Fig. 9 Influence of temperature on fluoranthene fluorescence excited at 266 nm (**a**) and 355 nm (**b**) in nitrogen for different pressures. The signal S_f^{++} is normalized to the molar fraction, the absorption cross section and the reference value at 473 K

3.4 Quenching effects

Concerning the specific quenching effect on the fluoranthene fluorescence, four ambient gases are tested between 0.1–4 MPa: nitrogen, argon (inert gases), carbon dioxide (present in exhaust gas recirculation in IC engines) in the temperature range of 473–873 K and air at 473 K. No quenching effect is observed in carbon dioxide or argon, as shown in Fig. 10, where the evolution of the fluorescence quantum yield versus pressure is similar, with a significant increase between 0.1 and 1.5 MPa, followed a slight increase up to 4 MPa. The increase of the fluorescence signal is more marked in nitrogen, then in carbon dioxide, then in argon. On the other hand, the quenching effect is efficient in air where the fluorescence signal decreases strongly for a temperature of 473 K and the two excitation wavelengths, with a decrease of 80% between 0.1–2 MPa (cf. Fig. 11). The vibrational relaxation mechanisms are in competition with the quenching phenomenon due to reactions between oxygen and fluoranthene molecules involving intersystem crossing in competition with fluorescence. The quenching effects on the fluorescence emission are studied at oxygen mole fractions between 0 and 20% at 473 K. As observed in Fig. 12,

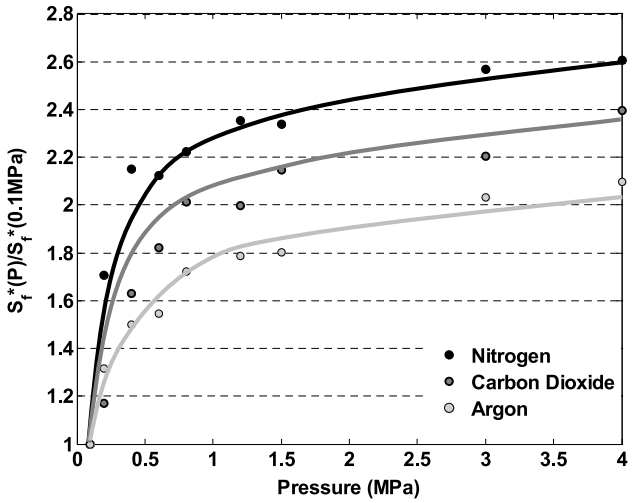

Fig. 10 Evolution of the fluoranthene fluorescence versus pressure for different ambient gases at 673 K and 266 nm. The signal S_f^* is normalized to the molecular density and the reference value at 0.1 MPa

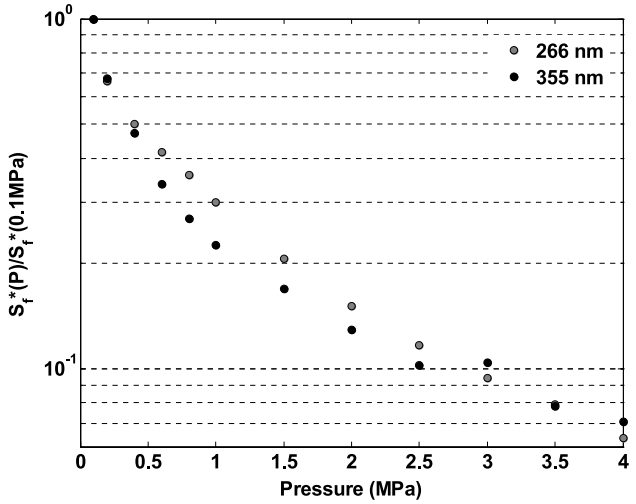

Fig. 11 Evolution of the fluoranthene fluorescence versus pressure in air at 473 K for the excitation wavelengths of 266 and 355 nm. The signal S_f^* is normalized to the molecular density and the reference value at 0.1 MPa

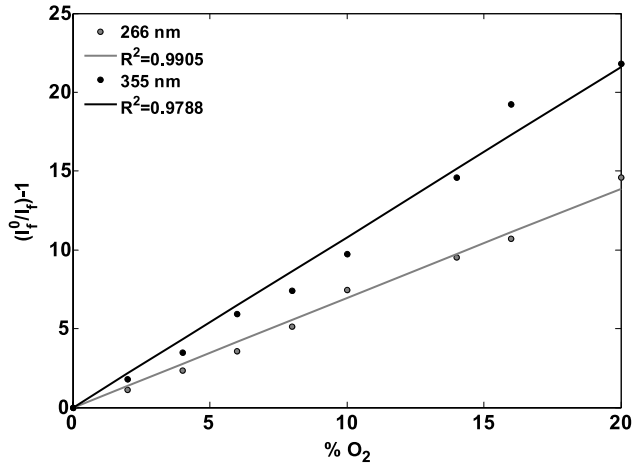

Fig. 12 Stern–Volmer plots for the fluoranthene fluorescence at 473 K and 1 MPa for the excitation wavelengths of 266 and 355 nm

the quenching behavior is described closely by the Stern–Volmer relation, with a linear evolution of the fluorescence intensity versus the oxygen percent in nitrogen:

$$\frac{I_f^0}{I_f} = 1 + k_{SV}[O_2] \tag{15}$$

where I_f^0 and I_f are the fluorescence intensities in the absence and in the presence of oxygen respectively, k_{SV} represents the Stern–Volmer constant and is the product of the quenching rate constant and the fluorescence lifetime, $[O_2]$ is the concentration of the quencher molecule.

Ossler et al. [14] have observed similar results for the fluorescence of gas-phase PAHs (naphthalene, fluorene, anthracene and pyrene) which was considerably quenched by oxygen and followed a Stern–Volmer description only at low temperatures. At high temperatures where oxygen mixtures are reactive, a second-order dependence on the oxygen concentration was obtained. For toluene, Koban et al. [18] have found non-linear Stern–Volmer plots at all studied temperatures between 300 and 650 K for the excitation wavelength of 248 nm and for temperature above 500 K for 266 nm excitation. This is attributed to the growing impact of internal conversion at elevated temperatures or short excitation wavelengths. Figure 12 shows the dependence of the quenching effect to the excitation wavelength, with a higher Stern–Volmer constant at 355 nm. Sassu et al. [19] have revealed similar results with a Stern–Volmer quenching constant of 41.3 L/mol at 270 nm against 113.4 L/mol at 320 nm when they have established the wavelength dependency of the oxygen quenching constants for the fluoranthene fluorescence excited between 240 and 332 nm.

3.5 Single- or dual-excitation wavelength technique for the temperature measurement

From the satisfactory temperature dependence of the fluoranthene fluorescence for the two excitation wavelengths of 266 and 355 nm, this tracer can be used for quantitative imaging of temperature in homogeneously or inhomogeneously flows. Three techniques can be applied: the single-color detection technique (cf. (2)) for homogeneously seeded systems, the single-excitation two-color detection technique (cf. (4)) and the dual-excitation wavelength technique (cf. (5)) for inhomogeneously seeded systems.

In order to determine absolute temperature, calibration curves, fits are deduced from previously results obtained in a large range of temperature and pressure (473–873 K and 0.1–4 MPa), in different ambient gases and for the two excitation wavelengths. Statistics are obtained from the accumulation of 300 fluorescence spectra. The average signal/noise ratio is equal to 42:1. According to the ambient gas and the pressure, the precision for the measurement temperature is between ±10–30 K for the single-color detection technique at 266 nm and between ±5–15 K at 355 nm, between ±36–80 K for the single-excitation two-color detection technique at 266 nm and between ±36–43 K at 355 nm, between ±35–65 K for the dual-excitation wavelength technique.

The first technique can be easily applied with a single point calibration in homogeneous concentration distributions of the tracer. Calibration curves can be calculated from the results presented previously for the fluoranthene fluorescence from 266 or 355 nm excitation. In order to obtain absolute temperatures, one condition of known temperature is sufficient. The curves presented in Fig. 9 are used to obtain the best fit to convert the fluorescence signal to temperature. An important temperature sensitivity is observed, with an exponential decrease by two orders of magnitude within

Table 2 Calibration fits for the temperature measurement from the single-color detection technique, valid in homogeneously seeded systems for 473–873 K temperature range, three pressures and ambient gases from fluoranthene fluorescence excited at 266 or 355 nm

		Argon	Nitrogen	Carbon dioxide
355 nm	0.1 MPa	$T = -84.417\ln(S_f) + 445.69$	$T = -81.236\ln(S_f) + 452.63$	$T = -81.311\ln(S_f) + 447.34$
		$R^2 = 0.9717$	$R^2 = 0.9821$	$R^2 = 0.9694$
	1.2 MPa	$T = -91.932\ln(S_f) + 442.64$	$T = -90.947\ln(S_f) + 445.9$	$T = -84.561\ln(S_f) + 444.72$
		$R^2 = 0.9619$	$R^2 = 0.9664$	$R^2 = 0.9633$
	4 MPa	$T = -93.972\ln(S_f) + 443.33$	$T = -86.288\ln(S_f) + 445.6$	$T = -89.233\ln(S_f) + 450.13$
		$R^2 = 0.9633$	$R^2 = 0.9638$	$R^2 = 0.9767$
266 nm	0.1 MPa	$T = -96.02\ln(S_f) + 450.93$	$T = -89.294\ln(S_f) + 452.91$	$T = -95.827\ln(S_f) + 454.22$
		$R^2 = 0.9824$	$R^2 = 0.9858$	$R^2 = 0.9876$
	1.2 MPa	$T = -104.54\ln(S_f) + 446.01$	$T = -110.01\ln(S_f) + 453.21$	$T = -110.4\ln(S_f) + 457.17$
		$R^2 = 0.969$	$R^2 = 0.9853$	$R^2 = 0.9899$
	4 MPa	$T = -109.27\ln(S_f) + 455.07$	$T = -110.08\ln(S_f) + 460.63$	$T = -107.39\ln(S_f) + 454.22$
		$R^2 = 0.9892$	$R^2 = 0.9893$	$R^2 = 0.9872$

the studied temperature range 473–873 K. Table 2 summarizes calibration fits valid for 473–873 K temperature range, three pressures and ambient gases from fluoranthene fluorescence excited at 266 and 355 nm. In comparison, Luong et al. [20] have determined the following calibration curve from the toluene LIF signal in atmospheric nitrogen flows:

$$T\,(\mathrm{K}) = -57.895\ln S_f + 289.08 \tag{16}$$

In the case of inhomogeneous tracer distribution, as during the mixing phase in IC engine, the single-excitation two-color detection technique can be applied by using one laser, two cameras and appropriate filters [20] or a single camera, a filter and mirror assembly [4] and by measuring simultaneously fluorescence in two wavelength regions. The sensitivity of the technique depends on the combination of chosen filters. A parametric study has been investigated to determine the optimal spectral bands. Figures 13 and 14 show the fluorescence ratio calculated from previous results for different spectral bands with 355 and 266 nm excitation. The two spectral wavelength bands which involve the highest ratio sensitivity are $\Delta\lambda_1 = 402$–424 nm and $\Delta\lambda_2 = 468$–490 nm. This combination corresponds to commercial band-pass filters called 410BP25 and 480BP25 (CVI Melles Griot). Calibration fits for the chosen filter combination are collected in Table 3. Temperature sensitivity of this technique is satisfactory with an increase of the ratio $S_f^{\Delta\lambda_1}/S_f^{\Delta\lambda_2}$ in argon at 1.2 MPa by 2.9 for the excitation wavelength of 355 nm and by 3 at 266 nm, between 473 and 873 K.

Concerning the dual-excitation wavelength technique, temperature can be inferred from the fluorescence ratio plotted in Fig. 15. Each point represents the ratio of the 266 nm

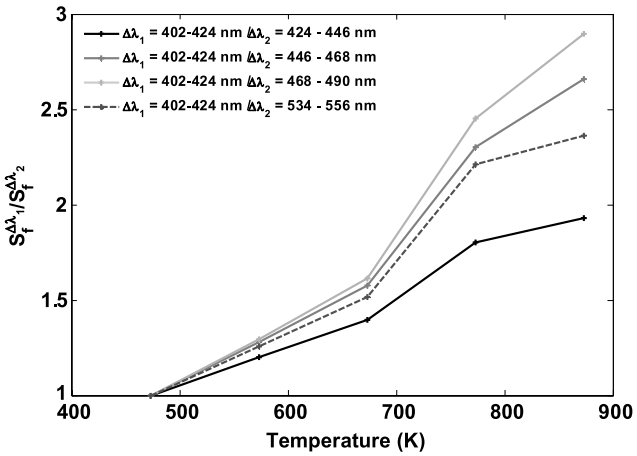

Fig. 13 Calibration curves for the single-excitation two-color detection technique obtained for different spectral bands from fluoranthene fluorescence excited at 355 nm in argon at 1.2 MPa

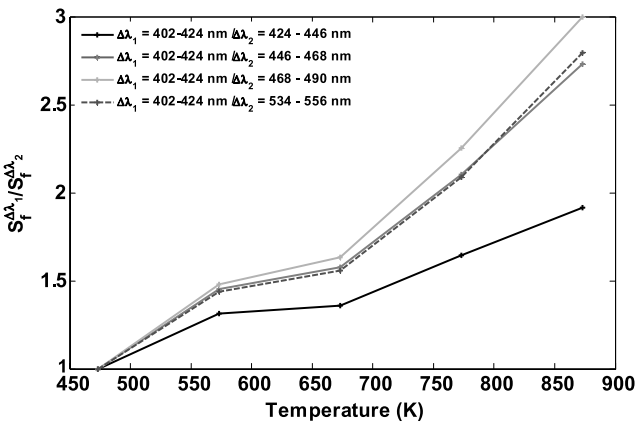

Fig. 14 Calibration curves for the single-excitation two-color detection technique obtained for different spectral bands from fluoranthene fluorescence excited at 266 nm in argon at 1.2 MPa

Table 3 Calibration fits of signal ratios $S_f^{\Delta\lambda_1}/S_f^{\Delta\lambda_2}$ for the temperature measurement from the single-excitation two-color detection technique, valid in inhomogeneously seeded systems for 473–873 K temperature range, three pressures and ambient gases from fluoranthene fluorescence excited at 266 or 355 nm. The signal ratio $S_f^{\Delta\lambda_1}/S_f^{\Delta\lambda_2}$ is detected for the two spectral bands: $\Delta\lambda_1 = 402$–424 nm and $\Delta\lambda_2 = 468$–490 nm

		0.2 MPa	1.2 MPa	4 MPa
355 nm	Argon	$0.3476\exp(0.0023T)$	$0.3295\exp(0.0024T)$	$0.3101\exp(0.0025T)$
		$R^2 = 0.9981$	$R^2 = 0.9938$	$R^2 = 0.996$
	Nitrogen	$0.2497\exp(0.0028T)$	$0.3019\exp(0.0026T)$	$0.3096\exp(0.0026T)$
		$R^2 = 0.9625$	$R^2 = 0.9946$	$R^2 = 0.9832$
	Carbon dioxide	$0.3049\exp(0.0026T)$	$0.3314\exp(0.0024T)$	$0.2877\exp(0.0027T)$
		$R^2 = 0.9652$	$R^2 = 0.9891$	$R^2 = 0.9988$
266 nm	Argon	$0.2983\exp(0.0026T)$	$0.3108\exp(0.0025T)$	$0.3444\exp(0.0023T)$
		$R^2 = 0.9917$	$R^2 = 0.9946$	$R^2 = 0.9935$
	Nitrogen	$0.2809\exp(0.0027T)$	$0.3004\exp(0.0026T)$	$0.3387\exp(0.0023T)$
		$R^2 = 0.9991$	$R^2 = 0.9985$	$R^2 = 0.9957$
	Carbon dioxide	$0.294\exp(0.0026T)$	$0.326\exp(0.0025T)$	$0.3196\exp(0.0025T)$
		$R^2 = 0.9914$	$R^2 = 0.9619$	$R^2 = 0.9932$

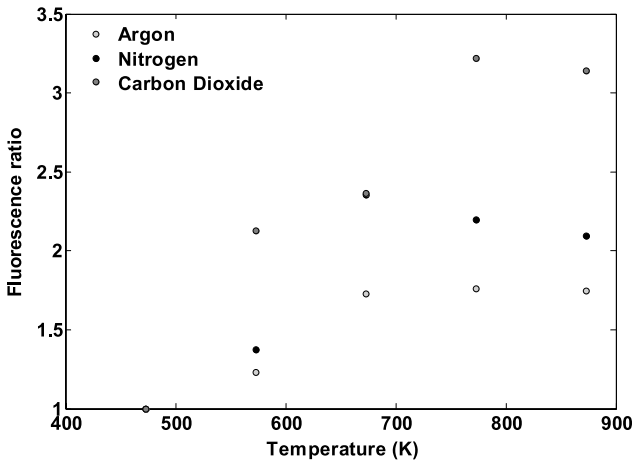

Fig. 15 Evolution of fluorescence signal ratios (266/355 nm) versus temperature in three ambient gases at 1.2 MPa

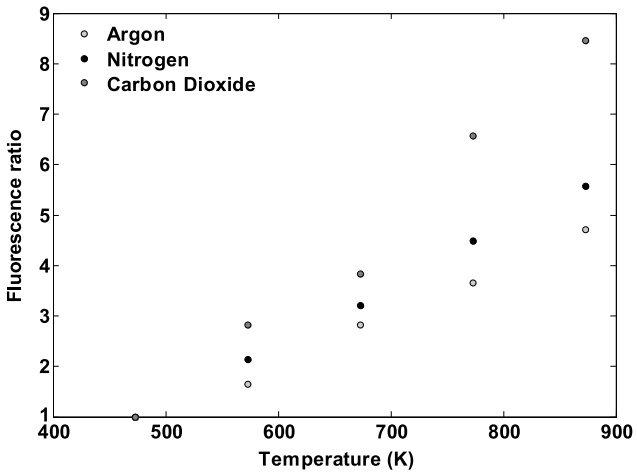

Fig. 16 Evolution of fluorescence signal ratios (266/355 nm) versus temperature in three ambient gases at 1.2 MPa by selecting two spectral bands ($\Delta\lambda_1 = 402$–424 nm at 266 nm and $\Delta\lambda_2 = 468$–490 nm at 355 nm)

fluorescence signal to the 355 nm signal for a given temperature. For the studied ambient gases and pressures, the fluorescence ratios show comparable sensitivity versus temperature, with a maximum increase at 1.2 MPa by about 3 in carbon dioxide between 473 and 873 K. However, the dual-excitation wavelength technique can be improved by selecting detection bands for each excitation wavelength to obtain a very sensitive ratio (cf. Fig. 16): $\Delta\lambda_1 = 402$–424 nm at 266 nm and $\Delta\lambda_2 = 468$–490 nm at 355 nm. In this case, temperature sensitivity is important with an increase of the fluorescence ratio by 8.5 in carbon dioxide, 5.6 in nitrogen and 4.7 in argon, between 473 and 873 K.

4 Conclusions

The influence of the pressure, temperature and gas composition on fluoranthene fluorescence has been characterized in a high-pressure and high-temperature facility for the two excitation wavelengths of 266 and 355 nm. This parametric study with a new combination, tracer and excitation wavelengths, is necessary to calibrate potential techniques for temperature measurements using fluoranthene.

Fluoranthene in iso-octane is chosen as tracer for its satisfactory spectroscopic properties at 266 and 355 nm. Absorption and fluorescence of fluoranthene are characterized for a pressure range of 0.1–4 MPa, a temperature range

of 473–873 K, a constant fluoranthene concentration of 3.099×10^{15} molecules·cm^{-3} in different ambient gases, nitrogen, argon, carbon dioxide and air.

As the absorption cross section increases strongly with temperature, the fluorescence signal has to be normalized by the corresponding cross section value to underline the temperature effect on the fluorescence. Fluoranthene presents a fluorescence emission band between 380–600 nm with a peak at 450 nm that corresponds to the fluorescence band $S_1 \rightarrow S_0$. For the studied temperatures and the two excitation wavelengths, the fluorescence signal increases with the pressure between 0.1–1.5 MPa to reach a constant value at high pressure. This evolution is attributed to the vibrational relaxation mechanisms favored when increasing pressure, which involve higher fluorescence quantum yields. The influence of the pressure on fluoranthene fluorescence is more marked at high temperature and for the excitation wavelength of 266 nm. A non-monotonous behavior of fluorescence signal versus pressure at high temperature is observed and is explained by high normalized standard deviations for these experimental points.

Concerning the influence of temperature, the fluorescence quantum yield decreases significantly with increasing temperature for the two excitation wavelengths and the studied pressure range. This evolution explains by the radiative mechanisms of intersystem crossing more efficient at high temperature. For example, at atmospheric pressure the fluorescence quantum yield decreases exponentially by two orders of magnitude in the studied temperature range. The quenching effect is very efficient in air where the fluorescence signal decreases strongly at 473 K. Moreover, the quenching behavior is described by the Stern–Volmer relation, when the oxygen concentration varies.

From these experimental results, temperature can be inferred from the fluorescence ratio according to the excitation wavelength and the detection band. Three techniques of temperature measurement are introduced: the single-color detection technique for homogeneously seeded flows, the single-excitation two-color detection technique and the dual-excitation wavelength technique for inhomogeneously seeded flows. Calibration curves are presented for the three techniques in a large domain of temperature, pressure and ambient gases, in conditions close to those encountered in engines, with the assumption where quasi-static results present a similar behavior to dynamic measurements in engine [21].

Acknowledgements M. Kühni was supported by a joint PhD grant from the French Ministry of Research.

This work was partly funded by the FUI (French Fond Unique Interministériel) in the framework of the MODELESSAIS Pôles de Compétitivité MOVE'O project, (www.pole-moveo.org) project number 07 2 90 6147.

References

1. C. Schulz, V. Sick, Prog. Energy Combust. Sci. **31**, 75 (2005)
2. A. Brauer, F. Beyrau, A. Leipertz, Appl. Opt. **45**, 4982 (2006)
3. S. Einecke, C. Schulz, V. Sick, Appl. Phys. B **71**, 717 (2000)
4. M. Luong, R. Zhang, C. Schulz, V. Sick, Appl. Phys. B **91**, 669 (2008)
5. W. Koban, J.D. Koch, R.K. Hanson, C. Schulz, Phys. Chem. Chem. Phys. **6**, 2940 (2004)
6. T. Fujikawa, K. Fukui, Y. Hattori, K. Akihama, in SAE Paper 2006-01-3366 (2006)
7. S.A. Kaiser, M.B. Long, Proc. Combust. Inst. **30**, 1555 (2005)
8. M.C. Thurber, PhD Thesis, Stanford University, 1999
9. J.D. Koch, PhD Thesis, Stanford University, 2005
10. M.C. Thurber, F. Grisch, R.K. Hanson, Opt. Lett. **22**, 251 (1997)
11. M.C. Thurber, R.K. Hanson, Exp. Fluids **30**, 93 (2001)
12. F. Grossmann, P.B. Monkhouse, M. Rider, V. Sick, J. Wolfrum, Appl. Phys. B **62**, 249 (1996)
13. V. Modica, C. Morin, P. Guibert, Appl. Phys. B **87**, 193 (2007)
14. F. Ossler, T. Metz, M. Alden, Appl. Phys. B **72**, 465 (2001)
15. K. Mimura, T. Madono, S. Toyama, K. Sugitani, R. Sugisaki, S. Iwamatsu, S. Murata, J. Anal. Appl. Pyrolysis **72**, 273 (2004)
16. D.L. Philen, R.M. Hedges, Chem. Phys. Lett. **43**, 358 (1976)
17. K.M. Bark, R.K. Forcé, Spectrochim. Acta **49**, 1605 (1993)
18. W. Koban, J.D. Koch, R.K. Hanson, C. Schulz, Appl. Phys. B **80**, 777 (2005)
19. L. Sassu, L. Perezzani, W.A. Ivancic, R.H. Barnes, B.W.A. Wabuyele, Appl. Spectrosc. **55**, 307 (2001)
20. M. Luong, W. Koban, C. Schulz, J. Phys. Conf. Ser. **45**, 133 (2006)
21. C. Morin, V. Modica, P. Guibert, Meas. Sci. Technol. **19**, 105105 (2008)